ESC European Society of Cardiology

Cardiovascular Research (2022) **118**, 3331–3345
https://doi.org/10.1093/cvr/cvac052

Neutrophil inhibition improves acute inflammation in a murine model of viral myocarditis

Paolo Carai [1,2], Laura Florit González[1,3], Stijn Van Bruggen [1], Valerie Spalart[1], Daria De Giorgio [1,4], Nadéche Geuens[1], Kimberly Martinod [1†], Elizabeth Anne Vincent Jones [1,2†], and Stephane Heymans [1,2*†]

[1]Centre for Vascular and Molecular Biology, Department of Cardiovascular Sciences, KU Leuven, Leuven, Belgium; [2]CARIM, Maastricht University, Maastricht, The Netherlands; [3]Department of Cardiology, Experimental Cardiology Laboratory, Utrecht University, Utrecht, The Netherlands; and [4]Department of Cardiovascular Medicine, Istituto di Ricerche Farmacologiche Mario Negri, IRCCS, Milan, Italy

Received 9 November 2021; revised 7 March 2022; accepted 24 March 2022; online publish-ahead-of-print 15 April 2022

Time of primary review: 16 days

Aims Viral myocarditis (VM) is an inflammatory pathology of the myocardium triggered by a viral infection that may cause sudden death or heart failure (HF), especially in the younger population. Current treatments only stabilize and improve cardiac function without resolving the underlying inflammatory cause. The factors that induce VM to progress to HF are still uncertain, but neutrophils have been increasingly associated with the negative evolution of cardiac pathologies. The present study investigates the contribution of neutrophils to VM disease progression in different ways.

Methods and results In a coxsackievirus B3- (CVB3) induced mouse model of VM, neutrophils and neutrophil extracellular traps (NETs) were prominent in the acute phase of VM as revealed by enzyme-linked immunosorbent assay analysis and immunostaining. Anti-Ly6G-mediated neutrophil blockade starting at model induction decreased cardiac necrosis and leucocyte infiltration, preventing monocyte and Ly6C^{High} pro-inflammatory macrophage recruitment. Furthermore, genetic peptidylarginine deiminase 4-dependent NET blockade reduced cardiac damage and leucocyte recruitment, significantly decreasing cardiac monocyte and macrophage presence. Depleting neutrophils with anti-Ly6G antibodies at 7 days post-infection, after the acute phase, did not decrease cardiac inflammation.

Conclusion Collectively, these results indicate that the repression of neutrophils and the related NET response in the acute phase of VM improves the pathological phenotype by reducing cardiac inflammation.

* Corresponding author. E-mail: s.heymans@maastrichtuniversity.nl
† These authors contributed equally.
© The Author(s) 2022. Published by Oxford University Press on behalf of the European Society of Cardiology.
This is an Open Access article distributed under the terms of the Creative Commons Attribution-NonCommercial License (https://creativecommons.org/licenses/by-nc/4.0/), which permits non-commercial re-use, distribution, and reproduction in any medium, provided the original work is properly cited. For commercial re-use, please contact journals.permissions@oup.com

Graphical Abstract

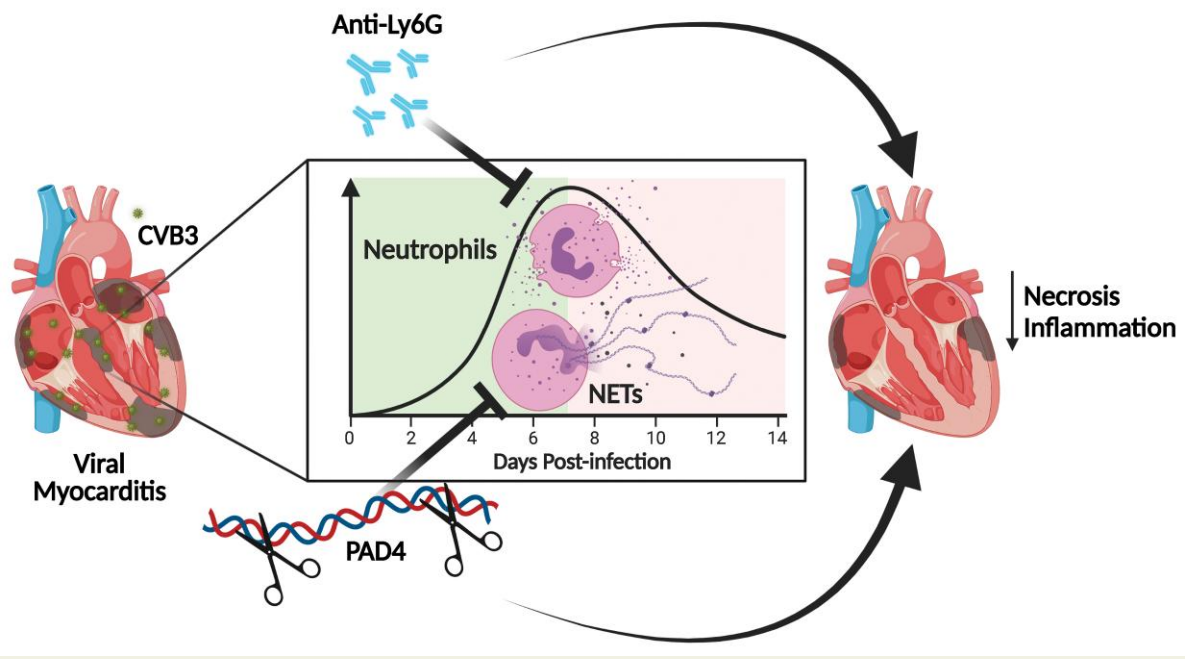

In CVB3-induced viral myocarditis, neutrophil or NET blockade before 7 days post-infection reduces cardiac necrosis and inflammation. CVB3, coxsackievirus B3; NET, neutrophil extracellular traps.

Keywords Viral myocarditis • Inflammation • Neutrophils • Neutrophil extracellular traps • Coxsackievirus B3

1. Introduction

Viral myocarditis (VM) is an inflammatory disease of the myocardium and may cause heart failure (HF) or sudden death in young adults.[1] A viral infection is the most common trigger of myocarditis worldwide:[2] enteroviruses (commonly coxsackievirus B3, CVB3) are the best-characterized cause of VM in humans and experimental animal models.[3] Despite being crucial to limiting the myocardium's viral infection, the host immune response can also be responsible for chronic cardiac damage in predisposed individuals.[4] Exaggerated leucocyte activation leads to myocardial dysfunction, with only 50% of the patients recovering from the pathology and 20% progressing to more severe dilated cardiomyopathy, and ultimately HF.[3] Current therapies for VM include HF medical care;[5] however, these treatments do not resolve the inflammatory aetiology. Corticosteroid-mediated immunodepression efficacy against VM has not been demonstrated yet. Moreover, this treatment may reignite the initial viral trigger,[3] making the need for tailored therapies in VM an urgent matter.

Neutrophils are the most abundant circulating immune cells. As the first line of defence against pathogens, they are vital members of the innate immune response in humans.[6] Furthermore, the release of chemokines and damage-associated molecular patterns by injured cardiomyocytes, activated resident macrophages, and endothelial cells allows for neutrophil recruitment to damaged or inflamed cardiac.[3,7,8] Upon activation, neutrophils release proteases, such as myeloperoxidase (MPO), and other anti-microbial proteins (defensins), secrete reactive oxygen species, and synthesize pro-inflammatory cytokines, further increasing the inflammatory response.[9] Moreover, neutrophils also have the unique ability to produce neutrophil extracellular traps (NETs), wherein decondensed nuclear DNA, histones, and other associated anti-microbial peptides act against pathogens.[10] However, neutrophil activation may also be detrimental in ischaemic heart disease and atherosclerosis[11,12] as well as during viral infections.[13] We hypothesized that decreasing neutrophil response, particularly NET release, may positively impact VM phenotype, and, thus, it could represent a new therapeutic strategy to investigate further.

2. Methods

2.1 Sources

All critical resources and materials (including experimental animals, cell lines, antibodies, and tools) are listed in *Table 1*, including the manufacturer and catalogue number (when applicable).

2.2 Animal experiments

2.2.1 Ethics approval and consent to participate

All experiments in this work involving the use of animals or isolation of primary cells from animals were monitored and approved by the KU Leuven Animal Ethics Committee, according to the Belgian law and the guidelines from Directive 2010/63/EU of the European Parliament, under the protocol n. 266/2015. Considering the influence that circadian rhythms exert on neutrophil biology,[14] all interventions on the animals have been performed during morning hours. Consent to participate is not applicable.

Table 1 List of key sources and materials

Reagent or resource	Source	Identifier
Antibodies and reagents		
TMB chromogen solution for ELISA	ThermoFisher Scientific	Cat# 002023
Cell Death Detection ELISA kit	Roche	Cat# 11544675001
Monoclonal mouse anti-DNA-peroxidase (Clone MCA-33)	Roche	Cat# 11 544 675 001
Monoclonal rat anti-mouse B220 V500	BD Biosciences	Cat# 561226
Monoclonal rat anti-mouse CD11b PE-Cy7	BD Biosciences	Cat# 552850
Monoclonal rat anti-mouse CD16/CD32	ThermoFisher Scientific	Cat# 14-0161-82
Monoclonal rat anti-mouse CD3 Pacific Blue	ThermoFisher Scientific	Cat# 48-0033-82
Monoclonal rat anti-mouse CD4 APC-H7	BD Biosciences	Cat# 560181
Monoclonal rat anti-mouse CD45 PerCp	Biolegend	Cat# 103130
Monoclonal rat anti-mouse CD8-FITC	ThermoFisher Scientific	Cat# 11-0081-85
Monoclonal rat anti-mouse F4/80 FITC	Biolegend	Cat# 123108
Monoclonal rat anti-mouse IgG	Bio x Cell	Cat# BE0089
Monoclonal rat anti-mouse Ly6C APC	Miltenyi	Cat# 130-123-796
Monoclonal rat anti-mouse Ly6G (Clone 1A8)	Bio x Cell	Cat# BE0075
Monoclonal rat anti-mouse Ly6G APC-Cy7	BD Biosciences	Cat# 560600
Monoclonal rat anti-mouse Ly6G	BD Biosciences	Cat# 551459
Monoclonal rat anti-mouse NK1.1 PE	BD Biosciences	Cat# 557391
Polyclonal donkey anti-Goat IgG AlexaFluor 488	ThermoFisher Scientific	Cat# A32814
Polyclonal donkey anti-Rabbit IgG AlexaFluor 568	ThermoFisher Scientific	Cat# A10042
Polyclonal goat anti-human/mouse MPO	R&D systems	Cat# AF3667
Polyclonal goat anti-rat IgG biotin	BD Biosciences	Cat# 559286
Polyclonal rabbit anti-human/mouse citrullinated Histone 3	Abcam	Cat# AB5103
Polyclonal rabbit anti-human/mouse MPO	ThermoFisher Scientific	Cat# PA5-16672
Rat monoclonal anti-mouse CD45	BD Biosciences	Cat# 553076
Streptavidin-Horse radish peroxidase conjugated	ThermoFisher Scientific	Cat# SA100-01
V-PLEX mouse cytokine/chemokine 19-Plex	Meso Scale Discovery	Cat# K15255D-1
Bacterial and virus strains		
CVB3 Nancy strain	ATCC	VR-30
Chemicals, peptides, and recombinant proteins		
Cell debris removal	Miltenyi	Cat# 130-109-398
Collagenase I	Merck	Cat# C0130
DAPI	Merck	Cat# D9542
Eosin	Merck	Cat# 861006
Formalin solution 37%	Merck	Cat# 104003
Harris-haematoxylin	VWR	Cat# 26041-06
Ionomycin	ThermoFisher Scientific	Cat# I24222
Percoll	Merck	Cat# P1644
PMA	Merck	Cat# P1585
Sudan Black B	Merck	Cat# 199664
Experimental models: organisms/strains		
Mouse: C3H/HeNHsd	Envigo	040; MGI:2160839
Mouse: B6(Cg)-Padi4tm1.2Kmow/J x B6.Cg-Tg(S100A8-cre,-EGFP) 1Ilw/J	KU Leuven	JAX Stock #026708, 7 generations backcrossed to C57BL/6J and then crossed with JAX Stock #021614
Mouse: B6(Cg)-Padi4tm1.2Kmow/J	KU Leuven	JAX Stock #026708, 7 generations backcrossed to C57BL/6J

2.2.2 Generation of neutrophil-selective peptidylarginine deiminase 4-deficient mice

B6.Cg-*Padi4*$^{tm1.2Kmow}$/J [peptidyl arginine deiminase 4, from now on, peptidylarginine deiminase 4 (PAD4$^{fl/fl}$)][15] mice were purchased from the Jackson Laboratory (USA) and crossed to C57BL/6J mice obtained from Charles River Laboratories (France) to reach seven generations of backcrossing to the C57BL/6J sub-strain. These mice were then intercrossed with B6.Cg-Tg(S100A8-cre, -EGFP)1Ilw/J (S100A8 is also known as migration inhibitory factor-related protein-8, MRP8, therefore, from now on MRP8-Cre-ires/GFP)[16] mice to obtain PAD4$^{fl/fl}$ x MRP8-Cre-ires/GFP mice (from now on, PAD4 Ne-KO). Background strain characterization by 128 single nucleotide polymorphism analyses revealed a 97.44% allelic match to the C57BL/6J sub-strain (Charles River Laboratories, USA). Colonies were maintained with one PAD4$^{fl/fl}$ x MRP8-Cre-ires/GFP parent crossed with a PAD4$^{fl/fl}$ mouse (from now on, PAD4 WT). Mice were genotyped for generic Cre expression using the following primer sequences: (Cre-F: GCG GTC TGG CAG TAA AAA CTA TC; Cre-R: GTG AAA CAG CAT TGC TGT CAC TT).

A priori sample size was determined using G*Power (3.1.9.4),[17] considering a *t*-test (means: difference between two independent means), an effect size $f = 1.40$ for the anti-Ly6G VM experiments, and $f = 0.81$ for the PAD4 WT and Ne-KO VM experiment, a level of significance $\alpha = 0.05$, and a power of 0.8 in a two-group setting.

2.2.3 VM timeline

Three- to four-week-old commercial C3H/HeNHsd male mice (Envigo, The Netherlands) were intraperitoneally injected with 10^7 $CCID_{50}$

(cell culture 50% infective dose) of CVB3 Nancy strain (VR-30, ATCC, USA) as previously described[18]

(VM) or 0.9% NaCl sterile solution (SHAM). Mice were euthanized at 4, 7, or 14 days post-infection (dpi, $n = 5$/per group).

2.2.4 Early acute neutrophil depletion in VM

Three- to four-week-old commercial C3H/HeNHsd male mice were intravenously injected with 200 µg of anti-Ly6G (Clone 1A8, BioXcell, USA) or isotype control antibody (ab). Twenty-four hours later, animals were intraperitoneally injected with 10^7 $CCID_{50}$ or 0.9% NaCl sterile solution. Anti-Ly6G or isotype control injections were repeated at 1 and 4 dpi. Mice were euthanized at 7 dpi for either histological analysis ($n = 10$ anti-Ly6G VM; $n = 10$ isotype control VM; $n = 5$ anti-Ly6G SHAM; $n = 5$ isotype control SHAM) or flow cytometry ($n = 6$/per group).

2.2.5 Late acute neutrophil depletion in VM

Three- to four-week-old commercial C3H/HeNHsd male mice were intraperitoneally injected with 10^7 $CCID_{50}$ or 0.9% NaCl sterile solution. Around 200 µg of anti-Ly6G or isotype control ab were intravenously injected at 7 and 11 dpi into the animals. Mice were euthanized at 14 dpi for either histological analysis ($n = 13$ anti-Ly6G VM; $n = 13$ isotype control VM; $n = 5$ anti-Ly6G SHAM; $n = 5$ isotype control SHAM) or flow cytometry ($n = 6$/per group).

2.2.6 Genetic NET ablation in VM

PAD4 WT littermates and 12- to 18-week-old PAD4 Ne-KO mice, with the same sex distribution, were intraperitoneally injected with 10^7 $CCID_{50}$ or 0.9% NaCl sterile solution. Mice were euthanized at 7 or 14 dpi for flow cytometry and histology analysis ($n = 11$ SHAM PAD4 WT; $n = 11$ SHAM PAD4 Ne-KO, $n = 10$ VM 7D PAD4 WT, and $n = 10$ VM 7D PAD4 Ne-KO, $n = 16$ VM 14D PAD4 WT, and $n = 21$ VM 14D PAD4 Ne-KO).

In all animal experiments described in this study, mice were anaesthetized with a 100 mg/kg ketamine and 10 mg/Kg xylazine intraperitoneal bolus. Sufficient sedation was verified by the absence of a paw withdrawal reflex. Then, the abdominal cavity was exposed, moving the intestines laterally. Around 800–1000 µL volume of whole blood was collected from the inferior vena cava with a 0.5 M EDTA-coated syringe. All animals were euthanized by bilateral pneumothorax and cardiac excision. Hearts were washed and exposed to a 1 M KCl solution to induce a homogenous end of cardiac activity in diastole. Cardiac tissue was either fixed in 10% neutral buffered formalin (NBF, Merck, Belgium) in PBS for at least 72 h at 4°C, flash-frozen in cryomedium (Merck), or processed for flow cytometry analysis.

2.3 MPO-DNA enzyme-linked immunosorbent assay

Plasma was isolated by centrifugation at 10 000 *g* of the whole blood previously collected and diluted 1:2 for analysis of MPO antigen. MPO-DNA complexes were measured using an in-house enzyme-linked immunosorbent assay (ELISA) modified from the Cell Death Detection ELISA (Roche, Switzerland). A 96-well Nunc immunoassay plate (MediSORP, Thermofisher Scientific, Belgium) was coated overnight with polyclonal anti-MPO antibody (1:1000 dilution, Thermofisher Scientific, Belgium) in 0.05 M sodium carbonate/sodium bicarbonate buffer (pH 9.6). After four washes with PBS containing 0.05% Tween-20 (Merck), wells were blocked with the assay incubation buffer. Samples were diluted in assay incubation buffer and incubated for 2 h. Following extensive washing, wells were incubated with mouse anti-DNA monoclonal antibody conjugated with peroxidase from the Roche Cell Death Detection ELISA, washed, and detected with ready-to-use 3,3′,5,5′-tetramethylbenzidine (TMB) substrate (Thermofisher Scientific, Belgium). The reaction was stopped with 1 N HCl, and the plate read at 450 nm wavelength using a Gen5 microplate reader (Biotek, France). A background correction was performed with a reading at 630 nM. Optical density values were then normalized to values obtained from a control plasma pool from healthy C57BL/6J mice (8 weeks of age, both sexes in equal amount), considered as a negative control. Sample concentrations were calculated using a sigmoidal interpolation of a standard curve generated as previously described.[19]

2.4 Histology and immunofluorescence

Paraffin-embedded NBF-fixed cardiac sections (4–5 µm) were either stained with Harris-haematoxylin (Avantor, Belgium) and Eosin (Merck) to evaluate cardiac necrosis or immunolabelled with anti-mouse CD45 (1:100 dilution) and tyramide signal amplification (Thermofisher Scientific, Belgium) to assess overall cardiac inflammation. Fresh frozen sections (10 µm) were immunolabelled with anti-mouse MPO (1:80) and anti-citrullinated histone H3 (R2 + 8+17, H3Cit, 1:400) and AlexaFluor®-labelled secondary antibodies (1:1500) to evaluate cells forming NETs. Background fluorescence was quenched with Sudan black 0.1% solution (Merck) for 10 min.

All antibodies mentioned in this paragraph are listed in *Table 1*. In all fluorescent-based immunolabelled sections, nuclei were counterstained with a 2.5 ng/mL DAPI solution (Merck).

2.5 Microscopy and quantification

A series of images taken at 5× magnification per heart section were assembled into one image using Axiovision's MosaiX function (Zeiss, Oberkochen, Germany). For immunophenotyping, images were acquired at magnifications of 20× or 40×, with 15–20 images per sample. All images were analysed with ImageJ software.[20]

Myocardial necrosis was determined as a percentage of the sum of the necrotic areas per total cardiac area, with the aid of a 500000 μm^2/square grid centred on the image.

Immunostainings were quantified per myocardial cross-sectional area, as previously described.[21] Briefly, immune cell phenotyping was either determined as the number of CD45-positive cells (leucocytes) per cardiac area or as the percentage of positive-stained area per cardiac area in the case of MPO-positive (neutrophils) or MPO-H3Cit-double-positive (NET-forming neutrophils).

2.6 Circulatory, cardiac, and bone marrow immune cell isolation

Mice were anaesthetized, and whole blood was collected as described in Section 2.2. The chest cavity was further revealed, and the right atrium was incised to allow any remaining blood to flow out. The heart was immediately perfused with 5 mL ice-cold 0.05% EDTA in PBS. The perfusion needle was inserted into the left ventricle. The right atria were severed, with the perfusion solution slowly washing away any residual blood from the cardiac and peripheral vasculature. Paleness of the coronary arteries and cardiac veins was visually verified before cardiac excision. Both atria were removed, and the ventricles were placed in ice-cold PBS, and afterwards minced, under sterile laminar flow, into a 1 mm^3 size piece with a surgical blade and placed in an enzymatic

solution containing 2.5 mg/mL collagenase (Merck) for 30 min at 37°C to isolate the immune cell cardiac population. Afterwards, the single-cell suspension was resuspended in a fresh complete RPMI medium (10% FBS, 1% penicillin-streptomycin, all from Thermofisher Scientific, Belgium) and 22.5% cell debris removal solution (Miltenyi Biotec, Nederlands) at 4°C. An equal volume of fresh-cold PBS was stratified on top of the cell suspension and centrifuged at 3000 *g* for 10 min at 4°C to separate mononuclear cells from cellular debris. After centrifugation, both the upper- and interphase were discarded. The lower layer containing the immune fraction was then rinsed with fresh-cold PBS. Tibias and femurs from both hind legs were aseptically dissected, cleaned of muscle tissue, and carefully severed proximally to each joint. Each bone was then flushed with a 1 mL sterile syringe attached to a 25 G needle and loaded with fresh complete RPMI medium. Collected bone marrow samples underwent one cycle of erythrocyte lysis with a hypotonic buffer, centrifuged at 1000 *g*, and washed with PBS. Blood samples underwent three cycles of erythrocyte lysis with a hypotonic buffer. Cells were centrifuged at 1000 *g* and washed with PBS. Finally, all the cell pellets were resuspended in 200 µl of flow cytometry buffer (0.1% BSA and 2 mM EDTA in PBS), and cells were counted using a Hemavet 950 Veterinary Analyzer (Drew Scientific, USA).

2.7 Flow cytometry analysis

The immune cell samples were blocked with Fc block (anti-mouse CD16/CD32, 1:100 dilution, Thermofisher Scientific, Belgium) for 30 min on ice. The samples were then washed with flow cytometry buffer (0.1% BSA, 2 mM EDTA in PBS) and centrifuged at 1000 *g* at 4°C for 3 min. The pellets were then stained with the fluorochrome-conjugated antibodies for 30 min on ice in the dark. Samples were again washed with flow cytometry buffer and centrifuged at 1000 *g* at 4°C for 3 min. Finally, all the samples were resuspended in 200 µL of flow cytometry buffer and analysed on a CANTO II flow cytometer (Becton-Dickinson Benelux, Belgium). All antibodies used in this procedure were used at 1:100 dilution/10^6 cells (*Table 1*).

Cells were gated on singlets and leucocyte ($CD45^+$ cells) subpopulations were defined as follows (Gating strategy represented in Supplementary material online, *Figure S1*): NK ($CD45^+$, $NK1.1^+$, $CD3^-$), NKT ($CD45^+$, $NK1.1^+$, $CD3^+$), B lymphocytes ($CD45^+$, $NK1.1^-$, $CD3^-$, $B220^+$), T cells ($CD45^+$, $NK1.1^-$, $CD3^+$, $B220^-$), T helper ($CD45^+$, $NK1.1^-$, $CD3^+$, $B220^-$, $CD4^+$, $CD8^-$), T cytotoxic ($CD45^+$, $NK1.1^-$, $CD3^+$, $B220^-$, $CD8^+$, $CD4^-$), neutrophils ($CD45^+$, $NK1.1^-$, $CD3^-$, $B220^-$, $CD11b^+$, $Ly6G^+$, SSC^{High}), monocyte subpopulations ($CD45^+$, $NK1.1^-$, $CD3^-$, $B220^-$, $CD11b^+$, $Ly6G^-$, SSC^{Low}, $F4/80^-$, $Ly6C^{High/Mid/Low}$), and macrophage subpopulations ($CD45^+$, $NK1.1^-$, $CD3^-$, $B220^-$, $CD11b^+$, $Ly6G^-$, $F4/80^+$, $Ly6C^{High/Mid/Low}$). Data were analysed using FCS Express 7 (DeNovo Software, CA, USA).

2.8 Cytokine multiplex assay

A panel of 19 cytokines was measured using a V-PLEX Mouse Cytokine 19-Plex assay and a MESO QuickPlex SQ 120 (Meso Scale Diagnostics, USA), according to the manufacturer's instructions. Briefly, plasma, isolated as previously described, was diluted either 1:4 or 1:8 in diluent #41 (present in the assay kit), transferred to the two plates included, and incubated for 2 h at room temperature. A standard curve containing a set of serial dilutions of known concentrations of the analytes was included for each plate. After three washes with PBS containing 0.05% Tween-20, wells were incubated for 2 h at room temperature with the detection antibodies included in the assay. Just before instrument reading, wells were rewashed and incubated with reading buffer to start a chemiluminescence reaction.

Chemiluminescence values for each well were recorded individually, and concentrations of each analyte were calculated using MSD Discovery workbench 4.0 (Meso Scale Diagnostics, USA) according to the manufacturer's instructions.

2.9 Neutrophil isolation and *in vitro* NET formation assay

Peripheral neutrophils from PAD4 WT and Ne-KO mice were isolated as previously described.[22] Briefly, blood was drawn into 15 mM EDTA, 1% ultra-low endotoxin BSA (1:2 vol/vol). After removal of plasma, cells were resuspended in PBS and layered onto a discontinuous Percoll gradient (78/69/52% made isotonic with the addition of 10X PBS, Merck). Samples were centrifuged for 30 min at 1500 *g* at room temperature, without brakes. Cells were collected from the 69/78% interface, and hypotonic lysis was performed. After counting, cells were resuspended in phenol red-free RPMI-1640 supplemented with 10 mM HEPES at a 2×10^5 cells/mL concentration. A total of 10^4 cells were plated per well in a Corning CellBind 96-well (Avontor, Belgium) cell culture plate and allowed to settle to the bottom of the wells for 20 min at 37°C, 5% CO_2. Stimulation was performed using 4 µM ionomycin (Thermofisher Scientific, Belgium) or 100 nM Phorbol 12-myristate 13-acetate (PMA, Merck) for 3.5 h, followed by fixation with 2% paraformaldehyde. After overnight fixation, cells were immune-stained with anti-Ly6G and anti-H3Cit antibodies. Images were acquired and analysed using ImageJ software, as described above. NET-forming neutrophils were quantified as a percentage of $H3Cit^+Ly6G^+$ neutrophils per total $Ly6G^+$ neutrophils.

2.10 Quantification and statistical analysis

All statistical analyses were performed using GraphPad Prism 9 (GraphPad Software, USA). Data are expressed as mean ± SEM. The normality of the distribution of all continuous variables was assessed using the Shapiro–Wilk test. In the timeline experiment, a one-way ANOVA with Tukey's correction was used. When comparing only two groups, an unpaired Student *t*-test was used if groups passed the normality test, while a Mann–Whitney *U* test was used otherwise. When comparing two variables simultaneously (including treatment and pathology), a two-way ANOVA with Tukey's correction was used if groups passed the normality test, whereas a Kruskal–Wallis test was used otherwise. A Fisher's exact test was used for the hemizygosity rate analysis in PAD4 WT and Ne-KO littermates. Graphical data were shown as mean values with error bars indicating the SEM. Two-sided *P*-values of <0.05 (*), <0.01 (**), or <0.001 (***); indicated significant differences between groups.

3. Results

3.1 In VM, neutrophil recruitment and NET production peak during the acute phase

We first performed a preliminary VM timeline to understand the dynamics of neutrophil recruitment and NET production in VM. Neutrophils in the circulation significantly increased after 7 and 14 days post-infection (dpi, *Figure 1A*) compared with uninfected sham controls; however, circulating MPO-DNA complexes, a sign of neutrophil activation and NET release, were already detectable at 4 days post-

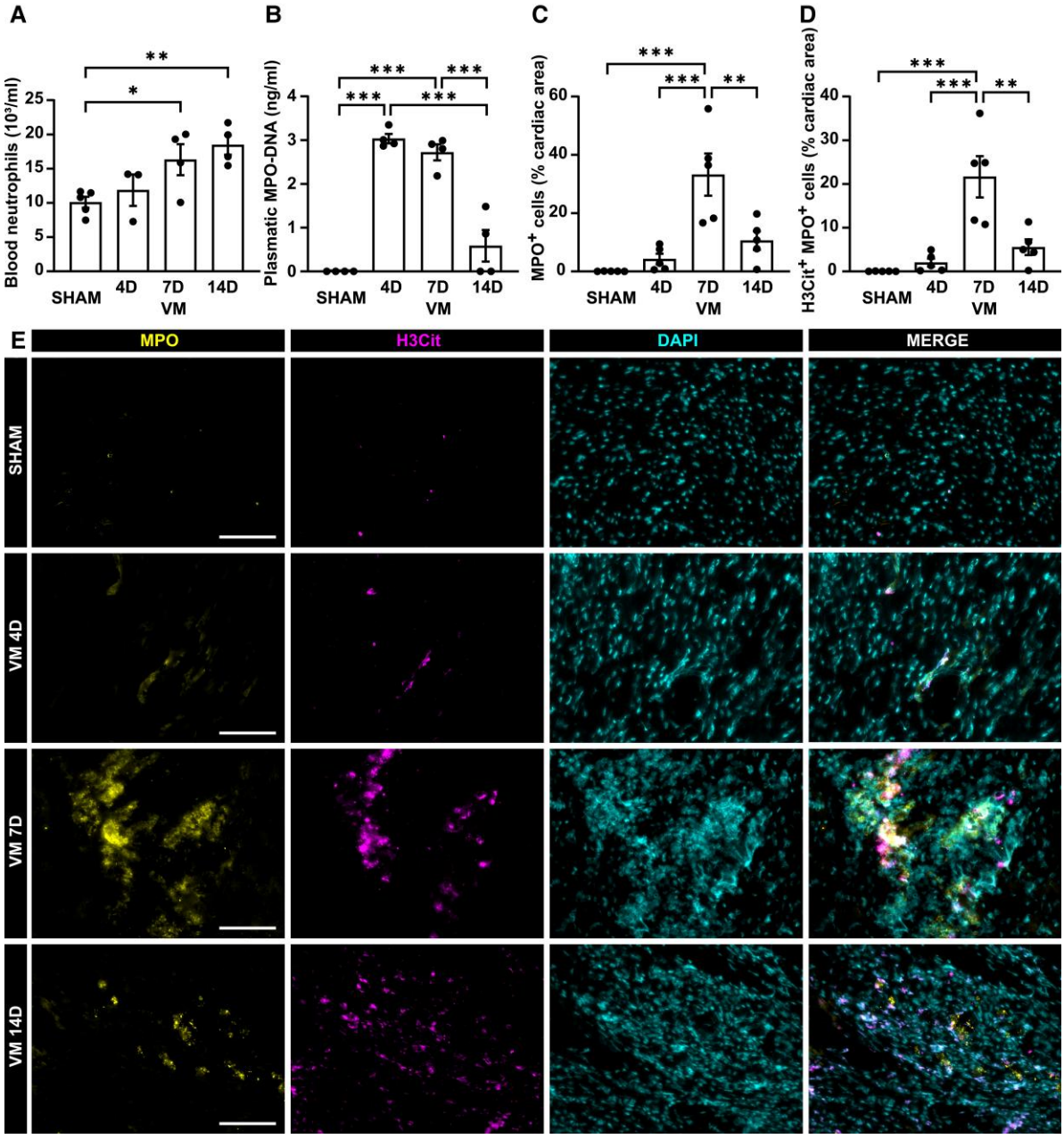

Figure 1 Neutrophil recruitment and NET formation peaks during the acute phase in CVB3-induced VM. (*A*) Circulating neutrophil levels measured by flow cytometry analysis in sham controls and VM at 4, 7, and 14 dpi ($n \geq 3$). (*B*) Circulating NETs during VM were measured as MPO-DNA complexes in the plasma of sham controls and VM at 4, 7, and 14 dpi by ELISA detection, $n = 4$. (*C–E*) Quantification and representative images of cardiac neutrophils (MPO^+, *C*) and NETs (MPO^+ $H3Cit^+$, *D*) in sham controls and VM at 4, 7, and 14 dpi. Murine cardiac sections were immune-stained for MPO, H3Cit, and counterstained with DAPI, $n = 5$. Scale bars = 100 μm. All values are expressed as mean ± SEM. Significance is assessed by one-way ANOVA, followed by Tukey's test: $^*P \leq 0.05$; $^{**}P \leq 0.01$; $^{***}P \leq 0.001$.

infection (*Figure 1B*) at the highest concentration, remaining detectable through 14 dpi. Accordingly, MPO-positive neutrophils in the infected hearts were present throughout the acute phase of VM (4–14 dpi, *Figure 1C–E*). MPO-positive cells infiltrated the heart, peaking at 7 dpi and eventually decreasing at 14 dpi (*Figure 1C* and *E*). Cardiac NETs, identified as MPO-positive and citrullinated histone 3 (H3Cit)-positive areas, peaked similarly at 7 dpi (*Figure 1D* and *E*), mainly localizing in VM lesions.

3.2 Early neutrophil depletion decreases cardiac monocyte recruitment and pro-inflammatory macrophage differentiation, improving VM-induced cardiac necrosis

We used an established model of anti-Ly6G-induced neutrophil depletion[23] to investigate whether neutrophils could pose a detrimental

role during the early inflammatory phase of VM (*Figure 2A*). Neutrophil depletion was confirmed in whole blood of sham controls and VM, although in the cardiac immune fraction, the reduction was not statistically significant upon infection ($P = 0.0529$, see Supplementary material online, *Figure S2A–B*). Anti-Ly6G treatment significantly reduced cardiac necrosis (*Figure 2B*) and prevented a significant increase of $CD45^+$ leucocytes in the myocardium upon CVB3 infection (*Figure 2C*), decreasing, at the same time, myocardial *CVB3* RNA genomes (see Supplementary material online, *Figure S2C*). The lack of neutrophils significantly altered, on its own, both innate and adaptive immunity, increasing circulatory NK T cells and cardiac T lymphocytes (see Supplementary material online, *Table S1*). Neutrophil ablation induced a significant accumulation of monocytes in the bone marrow, with a significant reduction in 'classical' $Ly6C^{High}$ phenotype (see Supplementary material online, *Figure S2D–E*), and in the circulation, without, however, affecting monocyte subtypes (see Supplementary material online, *Figure S2F–G*), in both sham and infected conditions. In contrast, anti-Ly6G treatment reduced the cardiac presence of monocytes (*Figure 2D–E*) without affecting their composition (*Figure 2F*). After neutrophil depletion, the total number of cardiac macrophages was not altered (*Figure 2D* and *G*); however, differentiation into 'classical' pro-inflammatory $Ly6C^{High}$ macrophages (*Figure 2H*) was severely reduced upon infection. The lack of neutrophils prevented the release of several pro-inflammatory cytokines and chemokines in the bloodstream (see Supplementary material online, *Table S2*). The treatment blocked the increase of chemokine (C-X-C motif) ligand 1 (CXCL1) and CXCL2 (*Figure 2I* and see Supplementary material online, *Table S2*, respectively). Both chemokines are considered murine functional homologues of human interleukin 8 (IL-8), crucial for neutrophil chemotaxis and activation through binding with CXC chemokine receptor 2 (CXCR2).[24] Moreover, in agreement with flow cytometry analysis, neutrophil depletion inhibited the secretion of chemokine (C-C motif) ligand 2 (CCL2, *Figure 2J*), also known as monocyte chemoattractant protein 1 (MCP1), and CXCL10 (*Figure 2K*), both prominent monocyte/macrophage chemotactic and activating molecules.[25,26]

Collectively, these data indicate a role for neutrophils in promoting a detrimental inflammatory response into the cardiac tissue during VM through the recruitment of pro-inflammatory leucocytes.

3.3 Neutrophil depletion after the acute phase does not improve VM-induced cardiac necrosis

Next, we investigated if neutrophil depletion could improve cardiac necrosis when the cardiac inflammatory response was already initiated (*Figure 3A*), at a stage equivalent to when VM patients are hospitalized. Anti-Ly6G treatment significantly reduced both circulatory and cardiac neutrophils in sham controls and VM (see Supplementary material online, *Figure S3A and B*). However, neutrophil ablation from 7 dpi did not reduce cardiac necrosis (*Figure 3B*) or myocardial *CVB3* RNA genomes (see Supplementary material online, *Figure S3C*), although still preventing a statistically significant increase of $CD45^+$ leucocytes in the myocardium (*Figure 3C*) compared with the control-treated group at 14 dpi. Neutrophil depletion from 7 dpi only marginally influenced circulatory and cardiac leucocyte composition (see Supplementary material online, *Table S3*). Late anti-Ly6G treatment neither induced a significant monocyte accumulation in the circulation after infection (see Supplementary material online, *Figure S3D and E*) nor reduced cardiac monocyte presence or composition (*Figure 3D–F*) or differentiation to macrophages (*Figure 3D, G,* and *H*). We surprisingly observed an increased cardiac monocyte presence (*Figure 3E*, left bars) in sham controls upon anti-Ly6G injection.

In summary, these data indicate that detrimental chemotaxis between neutrophils and monocytes is temporally restricted to the early acute phase of the inflammatory response during VM.

3.4 Genetic NET ablation reduces inflammation during acute VM and cardiac macrophage presence

Considering that blood and cardiac NET release (*Figure 1B* and *D*) followed the increasing neutrophil recruitment in VM (*Figure 1A* and *C*), we next investigated whether targeting NETs alone could alter the inflammatory response. For this purpose, we generated neutrophil-specific PAD4 knockout mice (PAD4 Ne-KO), crossing MRP8-Cre-ires/GFP[16] mice with $PAD4^{fl/fl}$ mice.[15] The observed MRP-Cre-ires/GFP hemizygosity rate in littermates was not different from the hypothetical 50%:50% Cre^+:Cre^- ratio (see Supplementary material online, *Figure S4A*). GFP detection by flow cytometry on whole blood confirmed specific Cre recombinase expression under *S100A8* (i.e. MRP8) promoter in neutrophils ($CD45^+$ $Ly6G^+$), minimal expression in other leucocyte subpopulations ($CD45^+$ $Ly6G^-$) of PAD4 Ne-KO mice, and no expression in any cell population of PAD4 WT (see Supplementary material online, *Figure S4B–C*). Ablation of PAD4 did not alter circulating leucocytes (see Supplementary material online, *Figure S4D–F*) but significantly reduced NET release upon neutrophil activation (see Supplementary material online, *Figure S4G*), confirming a crucial role for PAD4 in NET formation.[27]

In early acute VM (*Figure 4A*), lack of PAD4 in neutrophils decreased cardiac necrosis (*Figure 4B*), although not significantly, and cardiac inflammation (*Figure 4C*) at 7 dpi. Flow cytometry analysis of the cardiac immune fraction of PAD4 WT and Ne-KO littermates (see Supplementary material online, *Table S4*) showed a significantly reduced monocyte presence (*Figure 4D–E*) in the absence of NET formation upon VM, without influencing monocyte subpopulations (*Figure 4F*), circulating monocytes (see Supplementary material online, *Figure S4H–I*), or cardiac macrophages (*Figure 4D, G,* and *H*). In agreement with histological analyses, neutrophil-specific PAD4 deletion prevented a significant increase in systemic pro-inflammatory signals (see Supplementary material online, *Table S5*), neutrophil-activating factor CXCL1 (*Figure 4I*) and monocyte/macrophage activating CCL2 and CXCL10 (*Figure 4J* and *K*, respectively).

The improvements observed in the absence of NET formation were also validated in late acute VM (*Figure 5A*): histological analysis of infected PAD4 Ne-KO cardiac tissue confirmed a significant reduction in necrosis (*Figure 5B*) and inflammation (*Figure 5C*) compared with PAD4 WT hearts, without affecting CVB3 cardiac presence (see Supplementary material online, *Figure S4J*). Immune cell characterization showed persistent monocyte accumulation in the circulation in the absence of PAD4 upon VM (see Supplementary material online, *Figure S4K*) without altering the balance between monocyte subpopulations (see Supplementary material online, *Figure S4L*). Cardiac monocyte recruitment did not significantly change (*Figure 5D–F*). However, overall macrophage presence was strikingly decreased in the heart upon CVB3 infection (*Figure 5D* and *G*) with no changes in Ly6C-dependent subpopulations (*Figure 5H*) in infected PAD4 Ne-KO mice compared with WT littermates.

In summary, these results suggest that PAD4-dependent NETs are detrimental during the progression of CVB3-induced VM and that their presence is critical for monocyte/macrophage behaviour.

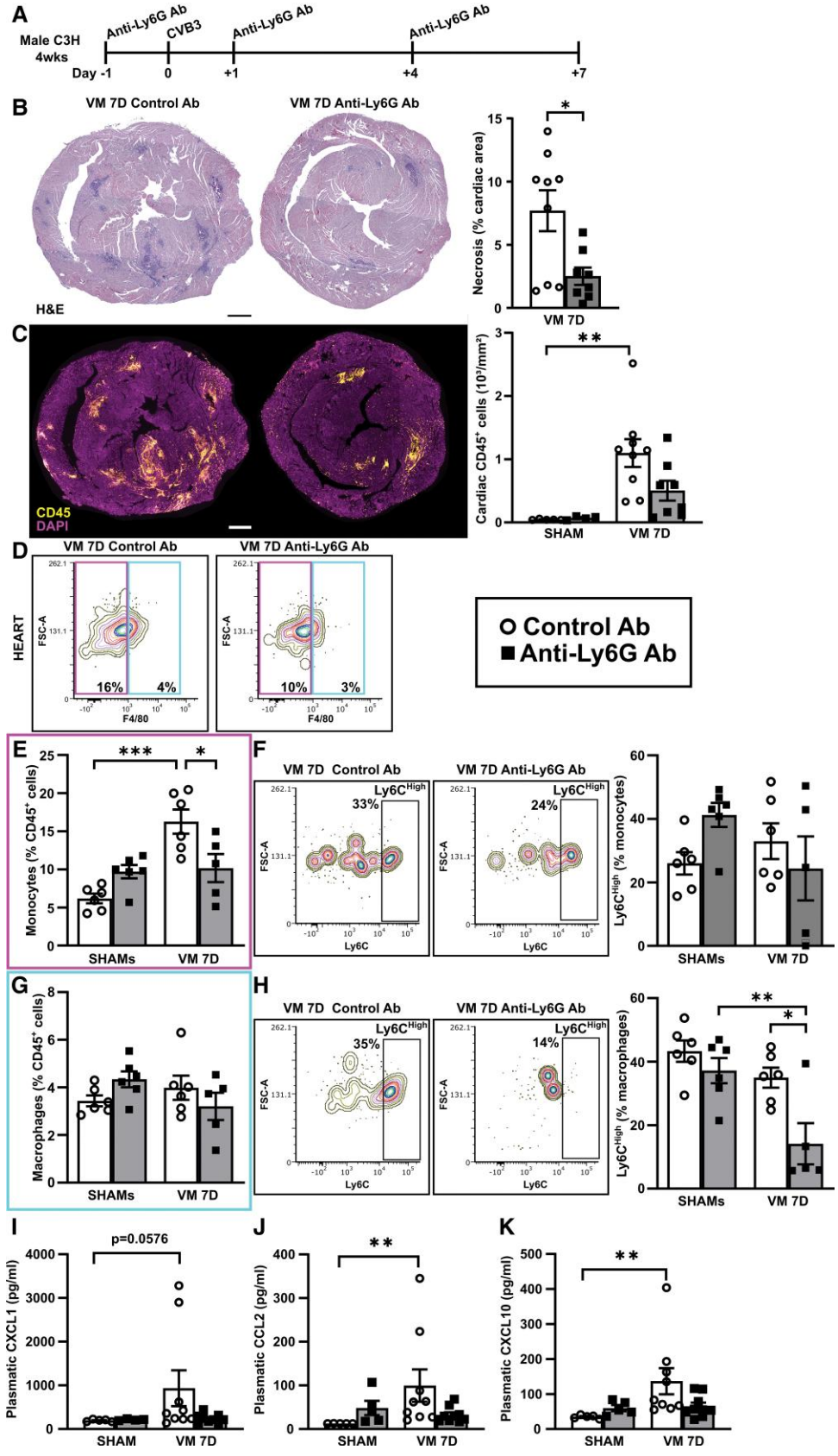

Figure 2 Early neutrophil depletion reduced cardiac inflammation in acute VM. (*A*) Experimental layout of anti-Ly6G-induced neutrophil depletion at 7 dpi. Representative images and quantification of cardiac necrosis (*B*), assessed by haematoxylin and eosin staining ($n \geq 8$), and cardiac inflammation (*C*, $CD45^+$ leucocytes, $n \geq 4$) in control and anti-Ly6G Ab-treated mice under sham or VM (7 dpi) conditions. Scale bars = 500 μm.

(continued)

Figure 2 Continued
Relative quantification of cardiac monocytes (Ly6G^{-}F4/80^{-}, Ly6C^{+}, *D* and *E*) and macrophages (Ly6G^{-} F4/80^{+} Ly6C^{+}, *D* and *G*) and pro-inflammatory Ly6C^{High} subpopulation (*F* and *H*, respectively) by flow cytometry analysis of the cardiac immune fraction of control and anti-Ly6G Ab-treated mice under sham or VM (7 dpi) conditions ($n \geq 5$). (*I–K*) Quantification of plasmatic concentrations of CXCL1 (*I*), CCL2 (*J*), and CXCL10 (*K*), assessed by multiplex ELISA assay in control and anti-Ly6G Ab-treated mice under sham or VM (7 dpi) conditions ($n \geq 5$). All values are expressed as mean ± SEM. Significance is assessed by an unpaired Student *t*-test for (*A*), Kruskal–Wallis test, followed by Tukey's test for (*I–K*), and by two-way ANOVA, followed by Tukey's test for the other panels: *$P \leq 0.05$; **$P \leq 0.01$; ***$P \leq 0.001$.

4. Discussion

This study reveals a prominent role for neutrophils in exacerbating the immune response in a CVB3-induced murine model of VM. Neutrophils and NET production peaked a week after CVB3 infection, and neutrophil blockade during the acute phase reduced cardiac necrosis and inflammation, preventing cardiac monocyte recruitment, Ly6^{High} pro-inflammatory macrophage differentiation, and pro-inflammatory cytokine signalling. Neutrophil depletion after this phase was not sufficient to improve the VM phenotype. Genetic PAD4-dependent NET inhibition from baseline was adequate to decrease cardiac necrosis and inflammation, monocyte recruitment, and subsequent differentiation into macrophages, also preventing the release of pro-inflammatory factors. Collectively, our results indicate that targeting neutrophil function and NET production may represent an early therapeutic strategy to prevent VM progression.

In our animal model, CVB3 infection induced massive neutrophil recruitment and NET production during the acute inflammatory phase of VM. In agreement with this, *in vitro,* human neutrophils can recognize and internalize CVB3 through Toll-like receptor 8 (TLR8),[28] an endosomal TLR specialized in detecting single-strand RNA viruses, such as CVB3.[29] Moreover, neutrophil-CVB3 interaction increases CD11b-mediated adhesion and migration, IL8 secretion, and NET release,[28] proving a direct effect of CVB3 on neutrophil recruitment and function during VM.

In our study, anti-Ly6G-mediated depletion highlighted a time-bound significant pro-inflammatory role for neutrophils during CVB3 infection. Our results disagree with the previous investigations[30] that deemed neutrophil contribution to the inflammatory response in VM less prominent compared with Gr-1^{+} cells (a combination of Ly6C/Ly6G epitopes, present in multiple cell lineages, such as neutrophils,[31] monocytes/macrophages,[31,32] myeloid-derived suppressor cells,[33] and T-cell subsets[31]). However, the effects that simultaneous depletion of multiple cell populations can have in the complex and multiphasic immune response of VM[3,34] should not exclude the contribution of neutrophils. In contrast, a more recent study confirmed a significant pro-inflammatory role of neutrophils in VM:[28] *in vitro* CVB3-activated neutrophils secreted several systemic pro-inflammatory cytokines such as IL1β, TNFα, and IL6, in agreement with what we observed in the plasma of neutrophil-depleted mice after early neutrophil depletion during VM. The same study observed a reduction in cardiac necrosis and viral titres upon neutrophil depletion *in vivo*, as we also did, thereby strengthening a possible role of neutrophils in viral dissemination. The authors did not observe major fluctuations in the other immune cell populations in the infected cardiac tissue of neutrophil-depleted animals. However, the limitations of the histological approach taken in that study (low cell counts) warranted further examination using flow cytometry. Despite these discrepancies, neutrophil activation, with the release of cytoplasmic granules (containing proteins such as cathepsin G, cathelicidin or LL37, and azurocidin) is known to activate monocytes, increasing vascular extravasation and permeability directly, and therefore monocyte recruitment.[35–37] Furthermore, activated neutrophils can secrete CCL2 through a non-canonical Wnt signalling pathway,[38] triggering monocyte recruitment and activation.[26] This phenomenon could explain the reduced monocyte influx in the heart observed after early neutrophil ablation upon infection, associated with the reduced levels of CCL2 in the plasma. Moreover, the CXCL1–CXCR2 axis, mouse homologue of the human IL-8-CXCR1 axis, not only is crucial for neutrophil recruitment, degranulation, NET release, both in an exocrine[39] and autocrine manner,[40] but in macrophages controls the secretion of inflammasome-dependent IL-1β.[41] In addition, macrophage exposure to azurocidin increases phagocytic activity and secretion of TNFα and IFNγ, hallmarks of a pro-inflammatory phenotype differentiation.[42,43] The release of neutrophil-derived CXCL10, a chemokine negatively associated with infectious and cardiovascular pathologies,[44] enhances macrophage proliferation through CXCR3 signalling, maintaining their inflammatory identity.[45,46] These findings agree with the reduction of Ly6C^{High} pro-inflammatory macrophages associated with CXCL10 plasmatic blockade that we observed upon anti-Ly6G treatment of CVB3-infected animals. However, neutrophil ablation after the acute phase did not improve VM, suggesting that prevention of neutrophil recruitment is favourable to the pathological outcome exclusively in the early phase of cardiac viral infection and inflammation before all the pro-inflammatory signals described take place. Neutrophils undergo apoptosis during the late stages of inflammation when they are cleared through macrophage-mediated efferocytosis.[47] This process promotes macrophage differentiation towards an anti-inflammatory phenotype, reinforcing a positive feedback loop that initiates the resolution of the immune response.[48] Accordingly, in our animal model, neutrophil blockade after their recruitment peak did not induce changes in cardiac macrophage presence or differentiation and did not translate into a reduction of cardiac damage compared with controls.

Finally, genetic inhibition of PAD4-dependent NETs was sufficient to reduce overall cardiac damage and inflammation and severely impair early monocyte recruitment and late macrophage presence. The NET formation is a complex process involving PAD4 activation, the citrullination of histones H3 and H4, and the release of neutrophil nucleosomes into the extracellular space together with serine proteases and other granule proteins.[49] This process has been associated with several cardiac pathologies such as atherosclerosis,[50] ischaemia–reperfusion injury,[51] and age-related cardiac fibrosis.[52] Recently, reducing NET release and increasing NET degradation in the acute phase improved the pathological outcome in experimental autoimmune myocarditis (EAM): both interventions decreased cardiac inflammation,[53] corroborating the outcome improvement we observed in CVB3-infected PAD4 Ne-KO mice. Under pathological conditions, NETs and their components reinforce not only pro-inflammatory functions of neutrophils, inducing a stronger IL-8 secretion,[54] but also monocyte/macrophage activation, differentiation, and phagocytic function, through the inflammasome pathway.[55] The inflammasome cascade triggers a positive feedback loop through

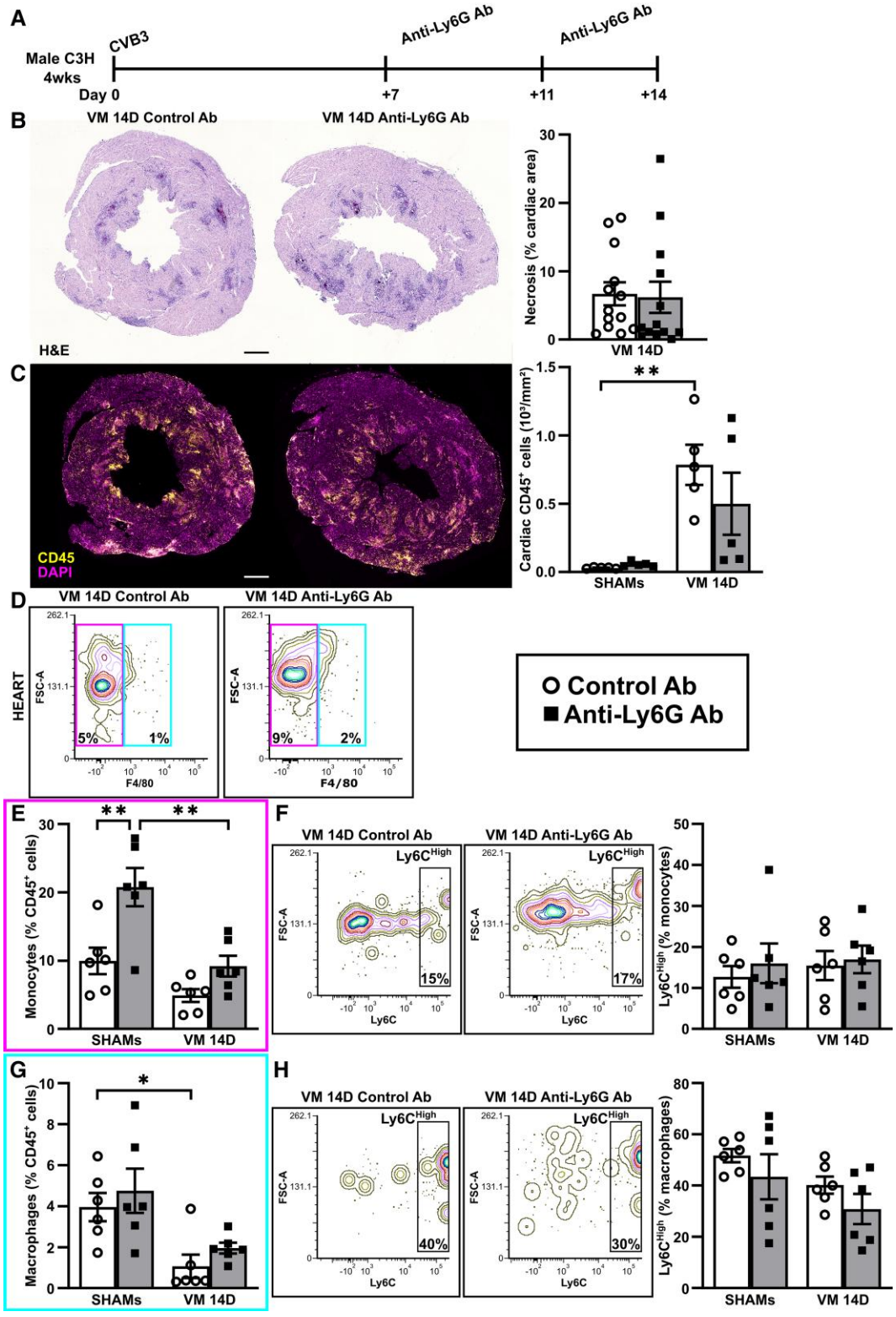

Figure 3 Neutrophil depletion after the acute phase does not improve VM-induced cardiac necrosis. (*A*) Experimental layout of anti-Ly6G-induced neutrophil depletion at 14 dpi. Representative images and quantification of cardiac necrosis (*B*), assessed by haematoxylin and eosin staining ($n = 13$), and cardiac inflammation (*C*, $CD45^+$ leucocytes, $n = 5$) in control and anti-Ly6G Ab-treated mice under sham or VM (14 dpi) conditions. Scale bars = 500 μm. Relative quantification of cardiac monocytes ($Ly6G^-$ $F4/80^-$ $Ly6C^+$, *D* and *E*) and macrophages ($Ly6G^-$ $F4/80^+$ $Ly6C^+$, *D* and *G*) and pro-inflammatory $Ly6C^{High}$ subpopulation (*F* and *H*, respectively) by flow cytometry analysis of the cardiac immune fraction of control and anti-Ly6G Ab-treated mice under sham or VM (14 dpi) conditions ($n = 6$). All values are expressed as mean ± SEM. Significance is assessed by an unpaired Student *t*-test for (*B*), and by two-way ANOVA, followed by Tukey's test for the other panels: $^*P \leq 0.05$; $^{**}P \leq 0.01$.

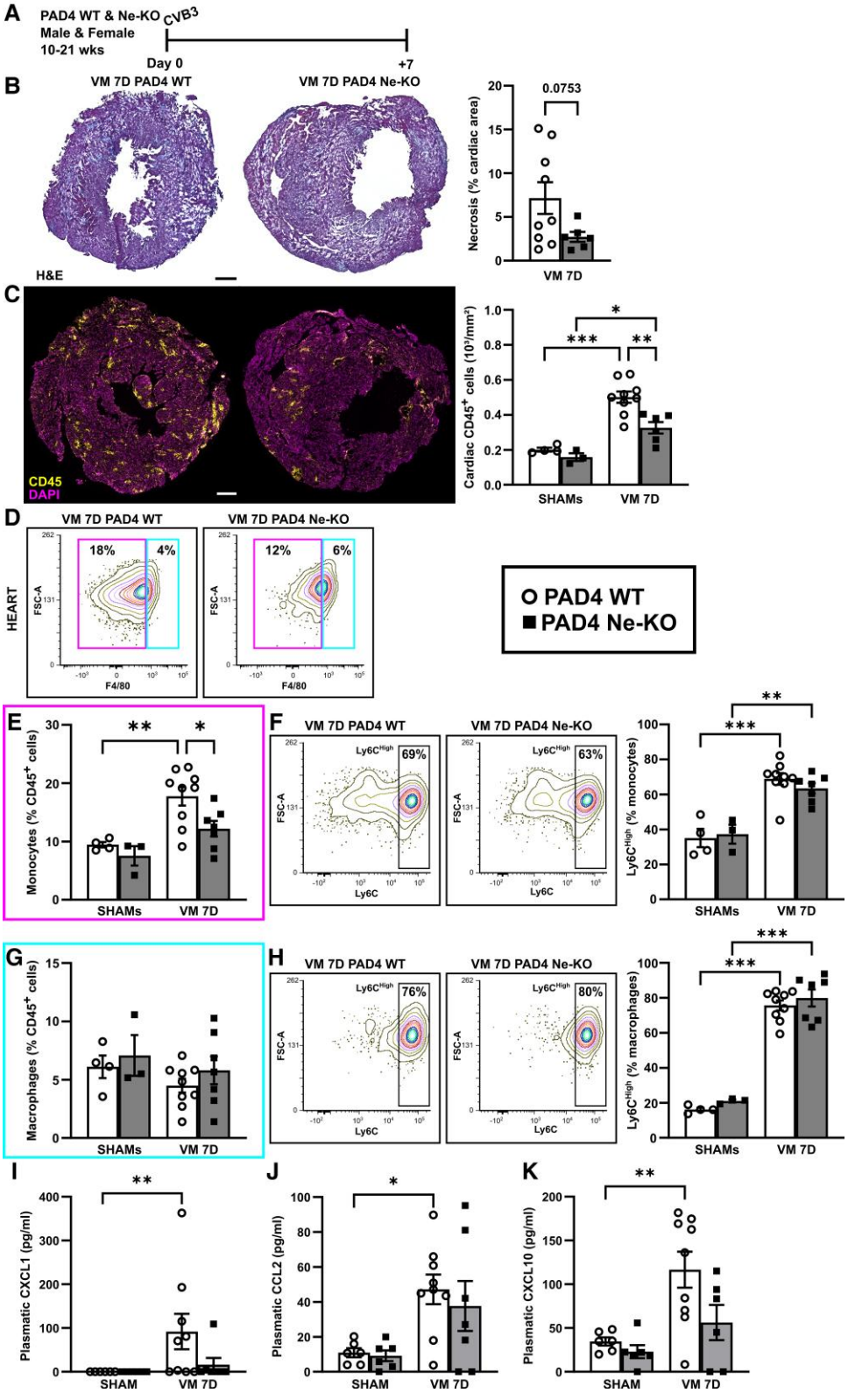

Figure 4 NET inhibition decreases monocyte recruitment during early acute VM. (*A*) Experimental layout of genetic NET inhibition at 7 dpi. Representative images and quantification of cardiac necrosis (*B*), assessed by haematoxylin and eosin staining ($n \geq 7$), and cardiac inflammation (*C*, $CD45^+$ leucocytes, $n \geq 7$) in PAD4 WT mice and Ne-KO littermates under sham and VM (7 dpi) conditions. Scale bars = 500 μm. Relative quantification of cardiac monocytes ($Ly6G^-$ $F4/80^-$ $Ly6C^+$, *D* and *E*) and macrophages ($Ly6G^-$ $F4/80^+$ $Ly6C^+$, *D* and *G*) and pro-inflammatory $Ly6C^{High}$ subpopulation (*F* and *H*, respectively) by flow cytometry analysis of the cardiac immune fraction of PAD4 WT mice and Ne-KO littermates under sham and VM (7 dpi) conditions ($n \geq 3$). (*I–K*) Quantification of plasmatic concentrations of CXCL1 (*I*), CCL2 (*J*), and CXCL10 (*K*), assessed by multiplex ELISA assay in PAD4 WT mice and Ne-KO littermates under sham or VM (7 dpi) conditions ($n \geq 6$). All values are expressed as mean ± SEM. Significance is assessed by a Mann–Whitney *U* test for (*B*), Kruskal–Wallis test, followed by Tukey's test for (*I*), and by two-way ANOVA, followed by Tukey's test for the other panels: $*P \leq 0.05$; $***P \leq 0.001$.

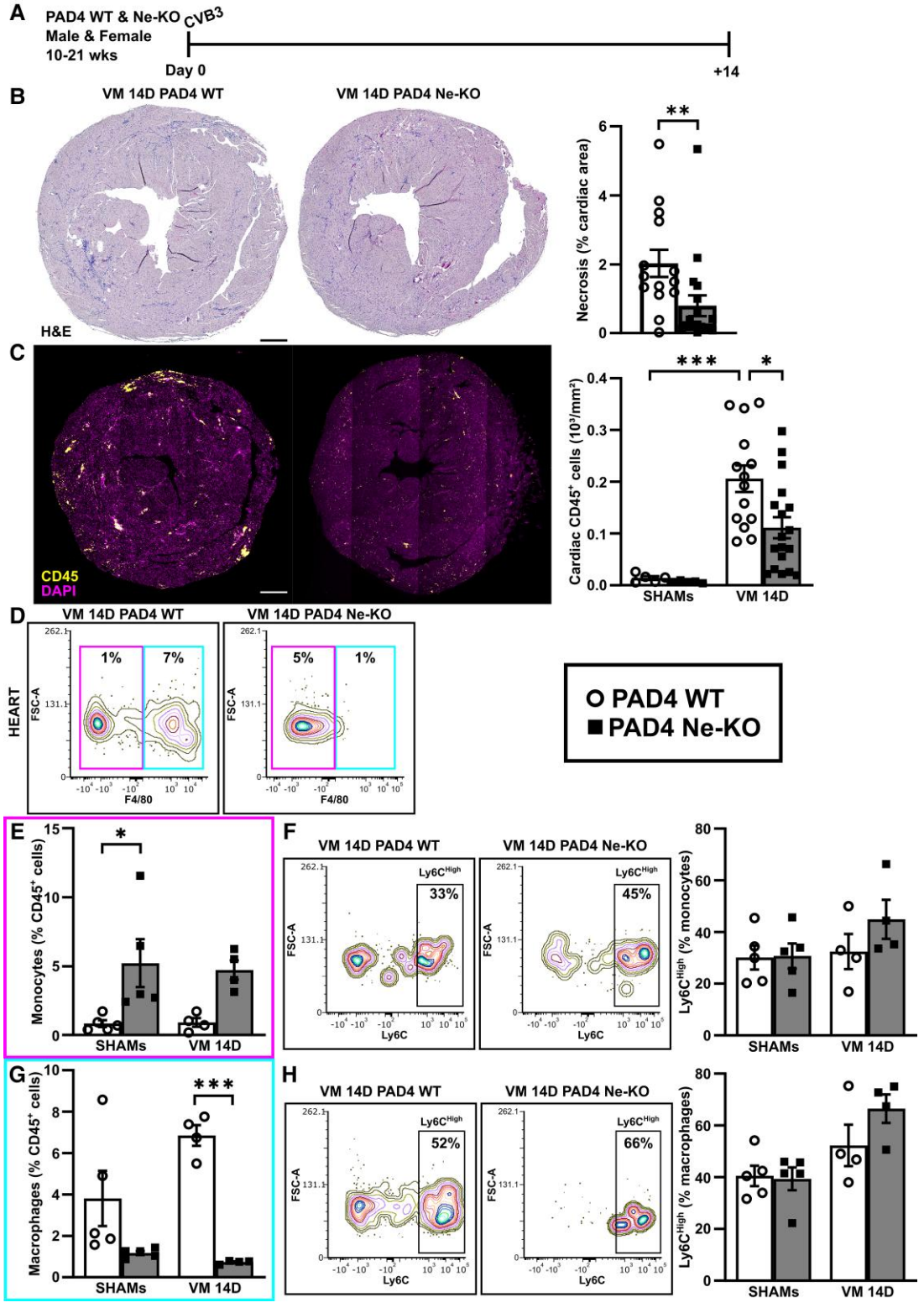

Figure 5 Lack of PAD4 reduces cardiac inflammation during late acute VM. (*A*) Experimental layout of genetic NET inhibition at 14 dpi. Representative images and quantification of cardiac necrosis (*B*), assessed by haematoxylin and eosin staining ($n \geq 14$), and cardiac inflammation (*C*, $CD45^+$ leucocytes, $n \geq 5$) in PAD4 WT mice and Ne-KO littermates under sham and VM (14 dpi) conditions. Scale bars = 500 µm. Relative quantification of cardiac monocytes ($Ly6G^-$ $F4/80^-$ $Ly6C^+$, *D* and *E*) and macrophages ($Ly6G^-$ $F4/80^+$ $Ly6C^+$, *D* and *G*) and pro-inflammatory $Ly6C^{High}$ subpopulation (*F* and *H*, respectively) by flow cytometry analysis of the cardiac immune fraction of PAD4 WT mice and Ne-KO littermates under sham and VM (14 dpi) conditions ($n \geq 4$). All values are expressed as mean ± SEM. Significance is assessed by a Mann–Whitney *U* test for (*A*), and by two-way ANOVA, followed by Tukey's test for the other panels: $*P \leq 0.05$; $***P \leq 0.001$.

the secretion of pro-inflammatory cytokines, such as TNFα, IL1β, IL6, and IL18,[55–57] which leads to even more neutrophil activation and degranulation, NET release, inflammatory monocyte and macrophage infiltration, tissue degradation, and myocardial damage. Accordingly, in our VM model, NET ablation by neutrophil-specific PAD4 deletion remarkably blocked the release of the same systemic pro-inflammatory cytokines and chemokines, directly reducing cardiac monocyte recruitment and macrophage presence, therefore confirming a detrimental effect of NET not only on neutrophil activation but also on monocyte and macrophage function during VM.

5. Limitations

Our study is not without limitations. One limitation in this study is represented by the differences in strain background, sex, and age between Ly6G-mediated neutrophil depletion and the PAD4 WT and Ne-KO VM experiments. Four-week-old male C3H mice used in the first set represent the gold standard for this model.[58–60] These mice possess high susceptibility to cardiac infection with minimal systemic disease and best resemble the higher VM prevalence in the male individuals and the cardioprotective effect of female hormones.[4]

Owing to time and feasibility constraints, we could not backcross the PAD4 WT and Ne-KO mice to a C3H background since the founder strains originated from two different C57BL/6 backgrounds, and a backcross to achieve a C57BL/6J background was already an extensive endeavour.[15,16] In addition, because of ethical concerns, we have used 12- to 18-week-old mice of both sexes, equally distributed among genotypes, in the second set of experiments. At 4 weeks of age, our in-house bred PAD4 colony does not reach a minimum acceptable weight of 20 g. In these conditions, mice have a higher mortality rate due to the gastrointestinal tropism of CVB3, thus unrelated to VM, compared with commercial C3H mice of the same age. Moreover, excluding female mice from our experiments would have been in disagreement with the 3R's principle.[61]

Another limitation is the lack of absolute quantification of isolated immune cells due to experimental constraints. However, as the main objective of this study was investigating relative changes in immune subpopulations, all flow cytometry analyses included are displayed as a percentage of $CD45^+$ leucocytes, except for Ly6C subsets.

Despite these limitations, anti-Ly6G-induced neutrophil depletion and genetic PAD4-dependent NET inhibition models displayed similar results upon CVB3 infection, supporting a detrimental role of neutrophil function during VM progression.

6. Conclusions

Collectively, neutrophils and NET blockade in the early acute phase improved VM-induced cardiac necrosis and reduced the cardiac immune response, influencing monocyte and macrophage function in the site of inflammation. Future confirmations of a beneficial role of neutrophil and NETs inhibition also at a later stage of VM are warranted, especially as a positive effect in other chronic cardiac pathologies has been already established.[50,52,53] Although the applicability of our findings might be challenged by the advanced pathological state of hospitalized VM patients, further investigation of the mechanisms underlying NET release, detection, and degradation by other members of the innate immune response might still represent a novel direction to pursue in the development of treatments preventing VM progression.

Supplementary material

Supplementary material is available at *Cardiovascular Research* online.

Authors' contributions

P.C., E.A.V.J., and S.H.: conceptualization; P.C., L.F.G., S.V.B., V.S., D.D.G., and N.G.: methodology; P.C., L.F.G., S.V.B., and D.D.G.: formal analysis; P.C.: investigation, data curation, visualization, and writing—original draft; K.M., E.A.V.J., and S.H.: resources; P.C.; P.C., L.F.G., S.V.B., V.S., D.D.G., N.G., K.M., E.A.V.J., and S.H.: writing—review and editing; K.M., E.A.V.J., and S.H.: supervision; P.C., K.M., E.A.V.J., and S.H.: project administration; K.M., E.A.V.J., and S.H: funding acquisition. All authors have read and approved the manuscript.

Acknowledgements

We are grateful to the laboratory members of Prof. Jones' and Prof. Martinod's groups in the Centre of Molecular and Vascular Biology, Department of Cardiovascular Science of the KU Leuven (Belgium), for the valuable scientific and technical assistance, especially to Dr S. Simmonds, Dr L. Gifre Renom, Ms L. Frederix, and Dr Sirima Kraisin.

Conflict of interest: S.H. receives personal fees for scientific advice to Astra-Zeneca, Cellprothera, CSL Behring, and Merck; unrestricted research grant from Pfizer. K.M. has received consulting fees for scientific advice to PEEL Therapeutics. All the remaining authors, P.C., L.F.G., S.V.B., V.S., D.D.G., N.G., and E.A.V.J., declare no competing interests.

Funding

This work was supported by the European Research Area Network on Cardiovascular Diseases (ERA-Net-CVD) MacroERA - 01KL1706 to P.C. and S.H. It was supported by a previous research grant from the Nederlandse Organisatie voor Wetenschappelijk Onderzoek (NWO) Vidi 91796338. Furthermore, we acknowledge the support of the Fonds Wetenschappelijk Onderzoek (FWO) G091018N and G0B5920N to S.H. and E.A.V.J., and 1514518N to K.M. which funded the generation of the NePAD4 mice.

Data availability

Additional data and materials will be individually shared upon reasonable request to the corresponding author.

References

1. Fabre A, Sheppard MN. Sudden adult death syndrome and other non-ischaemic causes of sudden cardiac death. *Heart* 2006;**92**:316–320.
2. Weintraub RG, Semsarian C, Macdonald P. Dilated cardiomyopathy. *Lancet* 2017;**390**:400–414.
3. Tschöpe C, Ammirati E, Bozkurt B, Caforio ALP, Cooper LT, Felix SB, Hare JM, Heidecker B, Heymans S, Hübner N, Kelle S, Klingel K, Maatz H, Parwani AS, Spillmann F, Starling RC, Tsutsui H, Seferovic P, van Linthout S. Myocarditis and inflammatory cardiomyopathy: current evidence and future directions. *Nat Rev Cardiol* 2021;**18**:169–193.
4. Corsten MF, Schroen B, Heymans S. Inflammation in viral myocarditis: friend or foe? *Trends Mol Med* 2012;**18**:426–437.
5. Ponikowski P, Voors AA, Anker SD, Bueno H, Cleland JGF, Coats AJS, Falk V, González-Juanatey JR, Harjola V-P, Jankowska EA, Jessup M, Linde C, Nihoyannopoulos P, Parissis JT, Pieske B, Riley JP, Rosano GMC, Ruilope LM, Ruschitzka F, Rutten FH, van der Meer P. 2016 ESC Guidelines for the diagnosis and treatment of acute and chronic heart failure. *E Heart J* 2016;**37**:2129–2200.
6. Colotta F, Re F, Polentarutti N, Sozzani S, Mantovani A. Modulation of granulocyte survival and programmed cell death by cytokines and bacterial products. *Blood* 1992;**80**:2012–2020.
7. Denning N-L, Aziz M, Sd G, Wang P. DAMPs and NETs in sepsis. *Front Immunol* 2019;**10**:2536.

8. Frantz S, Falcao-Pires I, Balligand JL, Bauersachs J, Brutsaert D, Ciccarelli M, Dawson D, de Windt LJ, Giacca M, Hamdani N, Hilfiker-Kleiner D, Hirsch E, Leite-Moreira A, Mayr M, Thum T, Tocchetti CG, van der Velden J, Varricchi G, Heymans S. The innate immune system in chronic cardiomyopathy: a European Society of Cardiology (ESC) scientific statement from the Working Group on Myocardial Function of the ESC. *Eur J Heart Fail* 2018;**20**:445–459.
9. Mantovani A, Cassatella MA, Costantini C, Jaillon S. Neutrophils in the activation and regulation of innate and adaptive immunity. *Nat Rev Immunol* 2011;**11**:519–531.
10. Sørensen OE, Borregaard N. Neutrophil extracellular traps - the dark side of neutrophils. *J Clin Invest* 2016;**126**:1612–1620.
11. Gaul DS, Stein S, Matter CM. Neutrophils in cardiovascular disease. *Eur Heart J* 2017;**38**: 1702–1704.
12. Sorvillo N, Cherpokova D, Martinod K, Wagner DD. Extracellular DNA NET-works with dire consequences for health. *Circ Res* 2019;**125**:470–488.
13. Schönrich G, Raftery MJ. Neutrophil extracellular traps go viral. *Front Immunol* 2016;**7**: 366.
14. Aroca-Crevillén A, Adrover JM, Hidalgo A. Circadian features of neutrophil biology. *Front Immunol* 2020;**11**:576.
15. Hemmers S, Teijaro JR, Arandjelovic S, Mowen KA. PAD4-mediated neutrophil extracellular trap formation is not required for immunity against influenza infection. *PLoS One* 2011;**6**:e22043.
16. Passegué E, Wagner EF, Weissman IL. JunB deficiency leads to a myeloproliferative disorder arising from hematopoietic stem cells. *Cell* 2004;**119**:431–443.
17. Faul F, Erdfelder E, Buchner A, Lang A-G. Statistical power analyses using G*Power 3.1: tests for correlation and regression analyses. *Behav Res Methods* 2009;**41**:1149–1160.
18. Rienks M, Papageorgiou A, Wouters K, Verhesen W, van Leeuwen R, Carai P, Summer G, Westermann D, Heymans S. A novel 72-kDa leukocyte-derived osteoglycin enhances the activation of toll-like receptor 4 and exacerbates cardiac inflammation during viral myocarditis. *Cell Mol Life Sci* 2017;**74**:1511–1525.
19. Vanderbeke L, van Mol P, van Herck Y, de Smet F, Humblet-Baron S, Martinod K, Antoranz A, Arijs I, Boeckx B, Bosisio FM, Casaer M, Dauwe D, de Wever W, Dooms C, Dreesen E, Emmaneel A, Filtjens J, Gouwy M, Gunst J, Hermans G, Jansen S, Lagrou K, Liston A, Lorent N, Meersseman P, Mercier T, Neyts J, Odent J, Panovska D, Penttila PA, Pollet E, Proost P, Qian J, Quintelier K, Raes J, Rex S, Saeys Y, Sprooten J, Tejpar S, Testelmans D, Thevissen K, van Buyten T, Vandenhaute J, van Gassen S, Velásquez Pereira LC, Vos R, Weynand B, Wilmer A, Yserbyt J, Garg AD, Matthys P, Wouters C, Lambrechts D, Wauters E, Wauters J. Monocyte-driven atypical cytokine storm and aberrant neutrophil activation as key mediators of COVID-19 disease severity. *Nat Commun* 2021;**12**:4117.
20. Schindelin J, Arganda-Carreras I, Frise E, Kaynig V, Longair M, Pietzsch T, Preibisch S, Rueden C, Saalfeld S, Schmid B, Tinevez J-Y, White DJ, Hartenstein V, Eliceiri K, Tomancak P, Cardona A. Fiji: an open-source platform for biological-image analysis. *Nat Methods* 2012;**9**:676–682.
21. Deckx S, Heggermont W, Carai P, Rienks M, Dresselaers T, Himmelreich U, van Leeuwen R, Lommen W, van der Velden J, Gonzalez A, Diez J, Papageorgiou A-P, Heymans S. Osteoglycin prevents the development of age-related diastolic dysfunction during pressure overload by reducing cardiac fibrosis and inflammation. *Matrix Biol* 2018;**66**:110–124.
22. Martinod K, Demers M, Fuchs TA, Wong SL, Brill A, Gallant M, Hu J, Wang Y, Wagner DD. Neutrophil histone modification by peptidylarginine deiminase 4 is critical for deep vein thrombosis in mice. *Proc Natl Acad Sci USA* 2013;**110**:8674–8679.
23. Christensen AD, Skov S, Haase C. The role of neutrophils and G-CSF in DNFB-induced contact hypersensitivity in mice. *Immunity Inflamm Dis* 2014;**2**:21–34.
24. Tecchio C, Micheletti A, Cassatella MA. Neutrophil-derived cytokines: facts beyond expression. *Front Immunol* 2014;**5**:508.
25. Ruytinx P, Proost P, van Damme J, Struyf S. Chemokine-induced macrophage polarization in inflammatory conditions. *Front Immunol* 2018;**9**.
26. Yoshimura T, Baba T, Midwood KS, Gschwandtner M, Derler R. More than just attractive: how CCL2 influences myeloid cell behavior beyond chemotaxis. *Front Immunol* 2019; **10**:2759.
27. Li P, Li M, Lindberg MR, Kennett MJ, Xiong N, Wang Y. PAD4 is essential for antibacterial innate immunity mediated by neutrophil extracellular traps. *J Exp Med* 2010;**207**: 1853–1862.
28. Rivadeneyra L, Charó N, Kviatcovsky D, de La Barrera S, Martín Gómez R, Schattner M, Charo N, Kviatcovsky D, de La Barrera S, Gómez RM, Schattner M. Role of neutrophils in CVB3 infection and viral myocarditis. *J Mol Cell Cardiol* 2018;**125**:149–161.
29. Heil F, Hemmi H, Hochrein H, Ampenberger F, Kirschning C, Akira S, Lipford G, Wagner H, Bauer S. Species-specific recognition of single-stranded RNA via toll-like receptor 7 and 8. *Science* 2004;**303**:1526–1529.
30. Xu D, Wang P, Yang J, Qian Q, Li M, Wei L, Xu W. Gr-1+ cells other than Ly6G+ neutrophils limit virus replication and promote myocardial inflammation and fibrosis following coxsackievirus B3 infection of mice. *Front Cell Infect Microbiol* 2018;**8**:157.
31. Egan CE, Sukhumavasi W, Bierly AL, Denkers EY. Understanding the multiple functions of Gr-1 + cell subpopulations during microbial infection. *Immunol Res* 2008;**40**:35–48.
32. Robben PM, LaRegina M, Kuziel WA, Sibley LD. Recruitment of Gr-1 + monocytes is essential for control of acute toxoplasmosis. *J Exp Med* 2005;**201**:1761–1769.
33. Bronte V, Brandau S, Chen S-H, Colombo MP, Frey AB, Greten TF, Mandruzzato S, Murray PJ, Ochoa A, Ostrand-Rosenberg S, Rodriguez PC, Sica A, Umansky V, Vonderheide RH, Gabrilovich DI. Recommendations for myeloid-derived suppressor cell nomenclature and characterization standards. *Nat Commun* 2016;**7**:12150.
34. Carai P, Papageorgiou AP, van Linthout DS, Velthuis S, Lutgens E, Wijnands E, Tschöpe C, Schmuttermaier C, Kzhyshkowska J, Anne E, Jones V, Heymans S. Stabilin-1 mediates beneficial monocyte recruitment and tolerogenic macrophage programming during CVB3-induced viral myocarditis. *J Mol Cell Cardiol* 2022;**165**:31–39.
35. Lee TD, Gonzalez ML, Kumar P, Grammas P, Pereira HA. CAP37, a neutrophil-derived inflammatory mediator, augments leukocyte adhesion to endothelial monolayers. *Microvasc Res* 2003;**66**:38–48.
36. Soehnlein O, Zernecke A, Eriksson EE, Rothfuchs AG, Pham CT, Herwald H, Bidzhekov K, Rottenberg ME, Weber C, Lindbom L. Neutrophil secretion products pave the way for inflammatory monocytes. *Blood* 2008;**112**:1461–1471.
37. Chertov O, Ueda H, Xu LL, Tani K, Murphy WJ, Wang JM, Howard OMZ, Sayers TJ, Oppenheim JJ. Identification of human neutrophil-derived cathepsin G and azurocidin/ CAP37 as chemoattractants for mononuclear cells and neutrophils. *J Exp Med* 1997; **186**:739–747.
38. Jung YS, Lee HY, Kim SD, Park JS, Kim JK, Suh P-G, Bae Y-S. Wnt5a stimulates chemotactic migration and chemokine production in human neutrophils. *Exp Mol Med* 2013;**45**: e27.
39. de Filippo K, Henderson RB, Laschinger M, Hogg N. Neutrophil chemokines KC and macrophage-inflammatory protein-2 are newly synthesized by tissue macrophages using distinct TLR signaling pathways. *J Immunol* 2008;**180**:4308–4315.
40. Capucetti A, Albano F, Bonecchi R. Multiple roles for chemokines in neutrophil biology. *Front Immunol* 2020;**11**:1259.
41. Boro M, Balaji KN. CXCL1 and CXCL2 regulate NLRP3 inflammasome activation via G-Protein–coupled receptor CXCR2. *J Immunol* 2017;**199**:1660–1671.
42. Soehnlein O, Kenne E, Rotzius P, Eriksson EE, Lindbom L. Neutrophil secretion products regulate anti-bacterial activity in monocytes and macrophages. *Clin Exp Immunol* 2007; **151**:139–145.
43. Soehnlein O, Kai-Larsen Y, Frithiof R, Sorensen OE, Kenne E, Scharffetter-Kochanek K, Eriksson EE, Herwald H, Agerberth B, Lindbom L. Neutrophil primary granule proteins HBP and HNP1–3 boost bacterial phagocytosis by human and murine macrophages. *J Clin Invest* 2008;**118**:3491–3502.
44. Altara R, Mallat Z, Booz GW, Zouein FA. The CXCL10/CXCR3 axis and cardiac inflammation: implications for immunotherapy to treat infectious and noninfectious diseases of the heart. *J Immunol Res* 2016;**2016**:1–12.
45. Ichikawa A, Kuba K, Morita M, Chida S, Tezuka H, Hara H, Sasaki T, Ohteki T, Ranieri VM, dos Santos CC, Kawaoka Y, Akira S, Luster AD, Lu B, Penninger JM, Uhlig S, Slutsky AS, Imai Y. CXCL10-CXCR3 enhances the development of neutrophil-mediated fulminant lung injury of viral and nonviral origin. *Am J Respir Crit Care Med* 2013;**187**:65–77.
46. Pandey V, Martinez AKF, Bastea LI, Döppler HR, Eisenhauer J, Le T, Edenfield B, Storz P. Cxcl10/cxcr3 signaling contributes to an inflammatory microenvironment and its blockade enhances progression of murine pancreatic precancerous lesions. *eLife* 2021;**10**: e60646.
47. Scannell M, Flanagan MB, deStefani A, Wynne KJ, Cagney G, Godson C, Maderna P. Annexin-1 and peptide derivatives are released by apoptotic cells and stimulate phagocytosis of apoptotic neutrophils by macrophages. *J Immunol* 2007;**178**:4595–4605.
48. Soehnlein O, Lindbom L. Phagocyte partnership during the onset and resolution of inflammation. *Nat Rev Immunol* 2010;**10**:427–439.
49. Papayannopoulos V. Neutrophil extracellular traps in immunity and disease. *Nat Rev Immunol* 2018;**18**:134–147.
50. Borissoff JI, Joosen IA, Versteylen MO, Brill A, Fuchs TA, Savchenko AS, Gallant M, Martinod K, ten Cate H, Hofstra L, Crijns HJ, Wagner DD, Kietselaer BLJH. Elevated levels of circulating DNA and chromatin are independently associated with severe coronary atherosclerosis and a prothrombotic state. *Arterioscler Thromb Vasc Biol* 2013;**33**: 2032–2040.
51. Savchenko AS, Borissoff JI, Martinod K, de Meyer SF, Gallant M, Erpenbeck L, Brill A, Wang Y, Wagner DD. VWF-mediated leukocyte recruitment with chromatin decondensation by PAD4 increases myocardial ischemia/reperfusion injury in mice. *Blood* 2014; **123**:141–148.
52. Martinod K, Witsch T, Erpenbeck L, Savchenko A, Hayashi H, Cherpokova D, Gallant M, Mauler M, Cifuni SM, Wagner DD. Peptidylarginine deiminase 4 promotes age-related organ fibrosis. *J Exp Med* 2017;**214**:439–458.
53. Weckbach LT, Grabmaier U, Uhl A, Gess S, Boehm F, Zehrer A, Pick R, Salvermoser M, Czermak T, Pircher J, Sorrelle N, Migliorini M, Strickland DK, Klingel K, Brinkmann V, Abu Abed U, Eriksson U, Massberg S, Brunner S, Walzog B. Midkine drives cardiac inflammation by promoting neutrophil trafficking and NETosis in myocarditis. *J Exp Med* 2019; **216**:350–368.
54. Dömer D, Walther T, Möller S, Behnen M, Laskay T. Neutrophil extracellular traps activate proinflammatory functions of human neutrophils. *Front Immunol* 2021;**12**.
55. Kahlenberg JM, Carmona-Rivera C, Smith CK, Kaplan MJ. Neutrophil extracellular trap–associated protein activation of the NLRP3 inflammasome is enhanced in lupus macrophages. *J Immunol* 2013;**190**:1217–1226.
56. Warnatsch A, Ioannou M, Wang Q, Papayannopoulos V. Neutrophil extracellular traps license macrophages for cytokine production in atherosclerosis. *Science* 2015;**349**: 316–320.
57. Chen W, Wang Q, Ke Y, Lin J. Neutrophil function in an inflammatory milieu of rheumatoid arthritis. *J Immunol Res* 2018;**2018**:1–12.

58. Corsten MF, Papageorgiou A, Verhesen W, Carai P, Lindow M, Obad S, Summer G, Coort SLM, Hazebroek M, van Leeuwen R, Gijbels MJJ, Wijnands E, Biessen EAL, de Winther MPJ, Stassen FRM, Carmeliet P, Kauppinen S, Schroen B, Heymans S. MicroRNA profiling identifies MicroRNA-155 as an adverse mediator of cardiac injury and dysfunction during acute viral myocarditis. *Circ Res* 2012;**111**:415–425.
59. Corsten MF, Heggermont W, Papageorgiou A-PP, Deckx S, Tijsma A, Verhesen W, van Leeuwen R, Carai P, Thibaut H-JJ, Custers K, Summer G, Hazebroek M, Verheyen F, Neyts J, Schroen B, Heymans S. The microRNA-221/-222 cluster balances the antiviral and inflammatory response in viral myocarditis. *Eur Heart J* 2015;**36**:2909–2919.
60. Deckx S, Johnson DM, Rienks M, Carai P, van Deel E, van der Velden J, Sipido KR, Heymans S, Papageorgiou A-P. Extracellular SPARC increases cardiomyocyte contraction during health and disease. *PLoS One* 2019;**14**:e0209534.
61. Bie P, Debrabant B. Gonadal sex and animal experimentation: perfection vs. 3R principle? *Basic Clin Pharmacol Toxicol* 2020;**127**:111–119.